Blind deconvolution of human brain SPECT images using a distribution mixture estimation

Max Mignotte [‡] [•] Jean Meunier [•]

[•] DIRO, Département d'Informatique et de Recherche Opérationnelle,
P.O. 6128, succ. Centre-ville, Montréal, Canada (Québec), H3C3J7.

[‡] INRIA, Institut National de Recherche en Informatique et Automatique, France.

ABSTRACT

Thanks to its ability to yield functionally-based information, the SPECT imagery technique has become a great help in the diagnostic of cerebrovascular diseases. Nevertheless, due to the imaging process, SPECT images are blurred and consequently their interpretation by the clinician is often difficult. In order to improve the spatial resolution of these images and then to facilitate their interpretation, we propose herein to implement a deconvolution procedure relying on an accurate distribution mixture parameter estimation procedure. Parameters of this distribution mixture are efficiently exploited in order to prevent overfitting of the noisy data or to determine the support of the object to be deconvolved when this one is needed. In this context, we compare the deconvolution results obtained by the Lucy-Richardson[1] method and by the recent blind deconvolution technique called the NAS-RIF algorithm[2] on real and simulated brain SPECT images. The NAS-RIF performs the best and shows significant contrast enhancement with little mottle (noise) amplification.

Keywords: Blind deconvolution, restoration, distribution mixture estimation, Markov Random Field, SPECT imaging.

1. INTRODUCTION

Single Photon Emission Computed Tomography (SPECT) images are obtained by the measure of radiations (gamma rays) coming from radioactive isotopes injected in the human body. Contrary to other medical imaging techniques, such as X-ray, Computer Tomography (CT), Magnetic Resonance Imaging (MRI), etc., this imagery process is able to give functionally rather than anatomically-based information, such as the metabolic behavior of organs, like the human brain, by measuring and visualizing the level of blood flow. This study of regional Cerebral Blood Flow (rCBF) can aid in the diagnostic of cerebrovascular diseases and brain disorders (e.g., Alzheimer's disease, Parkinson's disease, etc.) by indicating lower, or abnormal higher, metabolic activity in some brain regions.

Due to this imaging process, SPECT suffers from poor statistics and poor spatial resolution. Poor statistics result from the small number of photons that can be acquired for each image; principally owing to the low sensitivity of the collimator and the low dose of the injected radiopharmaceutical. Factors influencing the spatial resolution are mainly the scattering of the emitted photons and, to a lesser degree, the intrinsic resolution of the camera. Consequently, resulting cross-sectional SPECT images are very blurred and their interpretation by the nuclear physician is often labor-intensive and subjective. If the object to be visualized is small compared to the source-to-collimator distance, this degradation phenomenon may be considered to be approximately shift-invariant and, neglecting noise, this one can be modeled by a convolution process between the true undistorted image and the transfer function of the imaging system. A body of theoretical and experimental work has led to approximate this transfer function (also called the Point Spread Function or PSF) by a two-dimensional symmetric Gaussian function[3].[4] In order to improve the spatial resolution of SPECT images, some authors have thus investigated the SPECT image deblurring problem with this class of Gaussian transfer function and by using classical Wiener filter techniques.[3] This restoration procedure, also called a deconvolution procedure, is an important consideration in SPECT medical imaging where there may be localized singularities or cold/hot spots in the true image, associated with lesions or tumors. These localized singularities may not be visible in the blurred image, owing to the diffusive effects associated with the convolution

[1] Correspondence: Email:<mignotte,meunier>@iro.umontreal.ca.

process, which averages out differences in neighboring values. A deconvolution scheme could then be very useful in order to detect such singularities by improving the spatial resolution of SPECT images.

Under the assumption that the blur operation is exactly known, many methods have been investigated in the image processing community for tackling this deconvolution problem. Amongst the existing methods, the Lucy-Richardson (LR) algorithm[1] can efficiently take into account the Poisson noise phenomenon inherent to the SPECT imaging process. Nevertheless, this iterative algorithm requires a termination criteria in order to stop the procedure at the point where there is a balance between the fit to the image data and the amplification of the noise inherent to this problem. Let us note also that this deconvolution method remains limited and sensitive to the assumption made on the nature of the blurring function. In applications such as medical imaging, when little is known about the PSF, it can turn out often more relevant to estimate directly the PSF from the observed input image. This problem of simultaneously estimating the PSF (or its inverse) and restoring an unknown image is called "blind deconvolution". Recent techniques exist, such as the NAS-RIF algorithm,[2] and can be used efficiently in the SPECT imagery context.

In this paper, we propose to implement a deconvolution procedure in order to improve the spatial resolution of brain SPECT images. To this end, we first present an accurate distribution mixture parameter estimation which takes into account the diversity of the laws in the distribution mixture of a SPECT image. In our application, parameters of this distribution mixture are efficiently exploited in order to find a reliable stopping rule for the LR deconvolution algorithm. In this "supervised" deconvolution approach, we exploit also the two-dimensional Gaussian assumption for the PSF proposed by some authors,[3] .[4] Then, we will show that the joint estimation of the image and PSF can lead, thanks to the NAS-RIF algorithm, to better restoration results. For this blind deconvolution technique, in which the support of the object to be recovered is needed, we propose a novel support-finding algorithm using also the parameters of the aforementioned distribution mixture estimation procedure.

This paper is organized as follows. In Section 2, we detail the distribution mixture parameter estimation procedure. Section 3 briefly describes the LR and the NAS-RIF deconvolution methods. Deconvolution experimental results on real and simulated brain SPECT images are given in Sections 4.

2. MIXTURE PARAMETER ESTIMATION

Consider a couple of random fields $Z = (X, G)$, where $G = \{G_s, s \in S\}$ represents the field of observations located on a lattice S of N sites s (associated to the N pixels of the SPECT image), and $X = \{X_s, s \in S\}$ the label field (related to the N class labels of a segmented SPECT image). Each aforementioned label is associated to a specific brain anatomical tissue; the "CSF" area designates the region that is normally due to the lack of radiations. In this distribution mixture estimation problem, this region designates the brain region filled with Cerebrospinal Fluid (without blood flow and thus without radiation) and also the area outside the brain region. The "white matter" and "grey matter" (brightest region) are associated to a low and a higher level of blood flow respectively.[5] Each G_s takes its value in $\{0, \ldots, 255\}$ (256 grey levels), and each X_s in $\{e_1 = \text{"CSF"}, e_2 = \text{"white matter"}, e_3 = \text{"grey matter"}\}$.

The distribution of (X, G) is defined, firstly, by prior distribution $P_X(x)$, supposed to be Markovian and secondly, by the conditional likelihoods $P_{G_s/X_s}(g_s/x_s)$ whose shape and parameter vector $\Phi_{(x_s)}$ depends on the concerned class label x_s. In order to take into account the Poisson noise phenomenon inherent to the SPECT imaging process in the "CSF" area, we model $P_{G_s/X_s}(g_s/e_1)$, by a exponential law[4] with parameter α, namely; $(1/\alpha)\exp[-(g_s/\alpha)]$. To describe the brightness within the "white matter" and the "grey matter" regions, we model the conditional density function for these two regions by two different Gaussian laws.[4] The observable G is called the "incomplete data" whereas Z constitutes the "complete data".

In order to determine $\Phi = (\Phi_{(e_1)}, \Phi_{(e_2)}, \Phi_{(e_3)})$, we use the Iterative Conditional Estimation (ICE) algorithm. This estimation procedure[6] relies on an estimator $\hat{\Phi}(X, G)$ of the "complete data". This iterative method starts from an initial parameter vector $\Phi^{[0]}$ and generates a sequence of parameter vectors leading to the optimal parameters, in the least squares sense, with the following iterative scheme:

$$\Phi^{[p+1]} = \frac{1}{n}\left(\hat{\Phi}(x_{(1)}, g) + \cdots + \hat{\Phi}(x_{(n)}, g)\right)$$

where $x_{(i)}, i = 1, \ldots, n$ are realizations of X drawn according to the posterior distribution $P_{X/G}(x/g, \Phi^{[p]})$. In order to decrease the computational load, we can take $n = 1$ without altering the quality of the estimation.[6] Finally, we can

	ICE Procedure		
$\Phi^{\text{final}}_{(e_1)}$	$0.52_{(\pi)}$	$11_{(\alpha)}$	
$\Phi^{\text{final}}_{(e_2)}$	$0.26_{(\pi)}$	$100_{(\mu)}$	$648_{(\sigma^2)}$
$\Phi^{\text{final}}_{(e_3)}$	$0.22_{(\pi)}$	$172_{(\mu)}$	$383_{(\sigma^2)}$

Table 1. Estimated parameters for the picture reported in Fig. 4 (at bottom left). π stands for the proportion of the three classes within the SPECT image. α are the exponential law parameter. μ and σ^2 are the Gaussian law parameters.

use the Gibbs sampler algorithm[7] to simulate realizations of X according to the posterior distribution. For the local *a priori* model of the Gibbs sampler, we adopt an isotropic Potts model with a first order neighborhood.[8] In this model, there are two parameters denoted β_1, β_2, called "the clique parameters",[8] and associated to the horizontal and vertical binary cliques respectively †. Given this *a priori* model, the prior distribution $P_X(x)$ can be written as:

$$P_X(x) = \exp\left(-\sum_{<s,t>} \beta_{st}\big(1 - \delta(x_s, x_t)\big)\right)$$

where summation is taken over all pairs of neighboring sites and δ is the Kronecker delta function. In order to favor homogeneous regions with no privileged orientation in the Gibbs sampler simulation process, we choose $\beta_{st} = \beta_1 = \beta_2 = 1$. Finally, $\Phi^{[p+1]}$ is computed from $\Phi^{[p]}$ in the following way:

- **Stochastic Step**: using the Gibbs sampler, one realization x is simulated according to the posterior distribution $P_{X/G}(x/g)$, with parameter vector $\Phi^{[p]}$.
- **Estimation Step**: the parameter vector $\Phi^{[p+1]}$ is estimated with the Maximum Likelihood (ML) estimator of the "complete data" corresponding to each class:
  - If $N_1 = \#\{s \in S : x_s = e_1\}$ is the number of pixels of the "CSF" area, the ML estimator $\hat{\Phi}_{(e_1)}$ of α is given by[9]: $\hat{\alpha}(x, g) = (1/N_1) \sum_{s \in S : x_s = e_1} g_s$.
  - If $N_2 = \#\{s \in S : x_s = e_2\}$ and $N_3 = \#\{s \in S : x_s = e_3\}$ pixels are located in the "white matter" and "grey matter" regions respectively, the corresponding ML estimator of each class is given by the empirical mean and the empirical variance. For instance, for the "white matter" class, we have for $\hat{\Phi}_{(e_2)}$:

$$\hat{\mu}(x, g) = \frac{1}{N_2} \sum_{s \in S : x_s = e_2} g_s \qquad \hat{\sigma}^2(x, g) = \frac{1}{(N_2 - 1)} \sum_{s \in S : x_s = e_2} (g_s - \hat{\mu})^2$$

- Repeat until convergence is achieved; i.e., if $\hat{\Phi}^{[p+1]} \not\approx \hat{\Phi}^{[p]}$, we return to Stochastic Step.

Fig. 1 represents the estimated distribution mixture of the SPECT image shown in Fig. 4 (at bottom left). The three likelihoods $P_{G_s/X_s}(g_s/e_k)$, $k = 1, 2, 3$, weighted by the estimated proportion π_k of each class e_k, are superimposed to the image histogram. Corresponding estimates obtained by the estimation procedure, requiring about ten iterations, are given in Table 1.

3. DECONVOLUTION METHODS

In our application, the degradation of a SPECT image can be represented as the result of a convolution of the true image with a blurring function (the PSF) plus an additive term to model the noise from the physical system. If the imaging system is assumed to be linear and shift invariant, the degradation process can then be expressed by the following linear model:

$$g(x, y) = f(x, y) * h(x, y) + n(x, y)$$

†Cliques are subsets of site(s) which are mutual neighbors.[8]

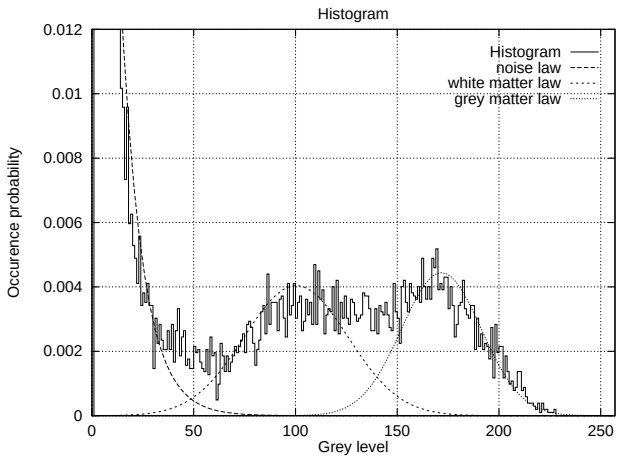

Figure 1. Image histogram of the picture reported in Fig. 4 (at bottom left) (solid curve) and estimated probability density mixture obtained with the ICE procedure (dotted and dashed curves).

where $g(x,y)$ is the degraded or blurred image, $f(x,y)$ is the undistorted true image, $h(x,y)$ is the PSF of the imaging system and $n(x,y)$ is the additive corrupting noise. In this notation, the coordinates (x,y) represent the discrete pixel locations, and $*$ is the discrete linear convolution operator. The problem is then to determine $f(x,y)$ given the observation $g(x,y)$.

The LR's algorithm

Assuming that the blurring function $h(x,y)$ is known, we can use the LR's algorithm.[1] This technique attempts to maximize the likelihood of the restored image by using the EM algorithm[10] when the image is assumed to come from a Poisson process. This iterative procedure may be succinctly expressed as:

$$\hat{f}_{k+1}(x,y) = \hat{f}_k(x,y)\left(h(-x,-y) * \frac{g(x,y)}{h(x,y) * \hat{f}_k(x,y)}\right)$$

In this form of notation, the division and the multiplication is done point-by-point.

The NAS-RIF algorithm

When little is known about the PSF, a solution for this deblurring problem consists in achieving a blind deconvolution technique. In the SPECT imagery context, the recent Non-negativity and Support constraints Recursive Inverse Filtering (NAS-RIF) technique[2] can be efficiently used. This blind deconvolution method is applicable to situations in which an object of finite support is imaged against an uniform or noisy background which is our case. It comprises a 2D variable Finite Impulse Response (FIR) filter $u(x,y)$ of dimension $N_x \times N_y$ with the blurred image pixels $g(x,y)$ as input. The output of this filter represents an estimate of the true image $\hat{f}(x,y)$. This estimate is passed through a nonlinear filter which uses a non-expansive mapping to project the estimated image into the space representing the known characteristics of the true image. The difference between this projected image $\hat{f}_{\text{NL}}(x,y)$ and $\hat{f}(x,y)$ is used as the error signal to update the variable filter $u(x,y)$. Fig. 2 gives an overview of this scheme. The image is assumed to be non-negative with known support. The cost function used in this restoration procedure is defined as:

$$\begin{aligned} J(u) &= \sum_{(x,y)\in\mathcal{D}_{\text{sup}}} \hat{f}^2(x,y)\left(\frac{1-\text{sgn}(\hat{f}(x,y))}{2}\right) \\ &+ \sum_{(x,y)\in\overline{\mathcal{D}}_{\text{sup}}} \left(\hat{f}(x,y) - L_{\text{B}}\right)^2 + \gamma\left(\sum_{\forall(x,y)} u(x,y) - 1\right)^2 \end{aligned}$$

where $\hat{f}(x,y) = g(x,y) * u(x,y)$, and $\text{sgn}(f) = -1$ if $f < 0$ and $\text{sgn}(f) = 1$ if $f \geq 0$. $\mathcal{D}_{\text{sup}}$ and $\overline{\mathcal{D}}_{\text{sup}}$ is the set of all pixels *inside* and *outside* the region of support respectively. The variable γ in the third term is nonzero only

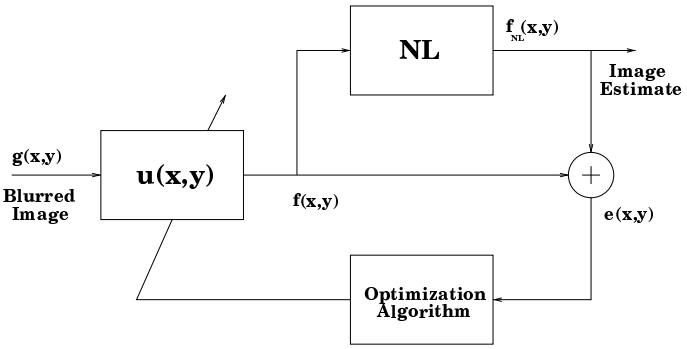

Figure 2. NAS-RIF algorithm.

when L_B is zero, i.e., the background color is black. The third term is used to constrain the parameter away from the trivial all-zero global minimum for this situation. Authors have shown that the above equation is convex with respect to $u(x, y)$, so that convergence of the algorithm to the global minimum is ensured using the conjugate gradient minimization routine.[2]

4. EXPERIMENTAL RESULTS

The effectiveness of these deconvolution schemes was tested on a cross-sectional phantom and several real brain SPECT images of 64×64 pixels size with 256 grey levels.

In order to stop the LR iterative procedure before the amplification of the noise, we decide to compute the parameters of the distribution mixture of $\hat{f}_k$ every 40 iterations. If the parameter associated to the background noise phenomenon (i.e., α) is above a fixed threshold, we decide to stop the procedure. Of course, this threshold has to be fixed empirically like the iteration number. Nevertheless, contrary to the iteration number, this strategy does not require a visual inspection for each iteration of the deconvolution procedure, that can be cumbersome and unreliable for an automatic deconvolution of a set of SPECT images.

In the case of the NAS-RIF algorithm, in which the rectangular support of the object to be restored is needed,[2] we exploit the parameters of the estimated distribution mixture of the input image g by adopting the following strategy; we assume that the row $\mathcal{R}_i \in S$ contains the object $\mathcal{O}$ to be deconvolved if we can find two consecutive sites $\in \mathcal{R}_i$ for which:

$$P(g_{ij}/''\text{CSF}'') \leq P(g_{ij}/''\text{white matter}'')$$

where the subscripts i, j refer to the pixel located at the i^{th} row and the j^{th} column and g to the luminance. We adopt an identical reasoning for the column and the object rectangular support is then determined by the set of pixels g_{ij} which belong to a row $\mathcal{R}_i$ and a column $\mathcal{C}_j$ containing the object $\mathcal{O}$. Fig. 3 displays examples of rectangular support determinations for some cross-sectional brain SPECT images.

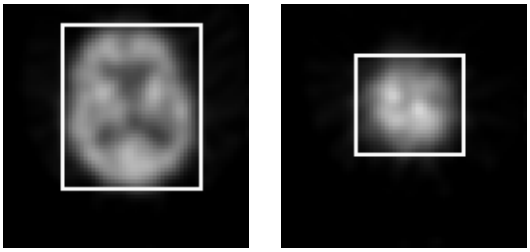

Figure 3. Examples of rectangular support determinations for some cross-sectional brain SPECT images.

For the LR algorithm, the initial estimated image is the original input image (i.e., $\hat{f}_0 = g$). Besides, the PSF is approximated by a two-dimensional Gaussian distribution with variance $\sigma^2 = 1.5$ (i.e., about 3 pixels of width at half maximum). This variance value has been chosen empirically, for each set of deconvolution experiments presented in this Section, in order to obtain the best "supervised" restoration results. The initial inverse FIR filter required by the NAS-RIF algorithm is simply the Kronecker delta function[2] and we have used $\gamma = 0$ because the background is not completely black. Finally, in order to objectively compare the spatial resolution improvements between the original and estimated image as well as the resolution of these two different deconvolution approaches, we have decided to stretch the histogram of the estimated image at convergence (i.e., $\hat{f}_{\text{final}}$) in order to get the same mean value as the original image g.

Fig. 4 gives examples of brain SPECT image deconvolutions. Computational cost is about 30 and 70 seconds on a standard Sun Sparc 2 workstation and for the LR and NAS-RIF algorithm respectively.

The effectiveness of these deconvolution techniques was also tested on a real SPECT phantom (i.e., a physical plexiglas head phantom filled with radioactive material and measured by a SPECT system) for which the ground truth of these segmented phantoms is exactly known and thus for which the performance of these methods can then be objectively judged. Fig. 5 presents examples of blind deconvolutions on a cross-sectional sliced SPECT phantom obtained by these two methods. We can notice that the original SPECT image is less blurred than the real ones previously processed (due to several factors such as a different dose of radioactive isotope contained in each uniform region of this SPECT phantom, a longer acquisition time, the stillness of this simulated brain during the SPECT process, etc.). In order to fully assess the success of this restoration procedure, we use the specific evaluation criteria proposed in,[11] based on the estimation of the two following measures:

(i) Firstly, the average contrast of the image, defined by $C = (1 - m_2/m_3)$, where m_2 and m_3 are the mean of the pixel value in the "white matter" and "grey matter" area respectively.

(ii) Secondly, the image mottle $M = \rho_2 M_2 + \rho_3 M_3$. M_2 and M_3 designate the ratio of the standard deviation of pixel values to the mean in the "white matter" and "grey matter" area respectively. ρ_2 and ρ_3 designate the proportion of pixel belonging to each class.

This last parameter allows to measure the amplification of the noise and/or measure the presence of undesirable artifacts that can be created by the deconvolution procedure in a uniform region of the real SPECT phantom. A reliable SPECT image restoration technique will then allow to enhance the contrast of the image with little increase in mottle, i.e., without amplifying too much the noise and/or without creating false artificial features (technically, an increase of 11%–14% of the original mottle of the image remains acceptable if the contrast enhancement is significantly increased[11]). Due to the difference of thickness between the cross-sectional slices of the real and segmented phantom, these abovementioned measures are estimated on the whole 3D phantom after this one has been registered[12] on the ground truth of the segmented phantom volume. The RL's method allows a contrast enhancement of 35.1% between the original and deconvolved SPECT phantom along with a barely acceptable amplification of the mottle of 14.9% whereas the NAS-RIF technique allows a contrast enhancement of 24.7% with a little and acceptable amplification of the mottle of 11.5%. This last result represents a significant improvement in image quality with a very small penalty and attest the validity of the NAS-RIF blind deconvolution method over the results obtained by a supervised deconvolution algorithm such as the LR's algorithm (see Fig. 6).

5. CONCLUSION

In this paper we have shown that a deconvolution procedure noticeably improves the spatial resolution of brain SPECT images and can be a great help to facilitate their interpretation by the nuclear physician. The proposed distribution mixture estimation procedure allows efficiently to give a reliable termination criteria for the unregularized iterative deconvolution techniques such as the LR algorithm or to accurately determine the rectangular support of the object to be restored for the NAS-RIF algorithm. This estimation procedure of the distribution mixture can be used for other applications such as an unsupervised Markovian segmentation of brain SPECT images or to give relevant information in order to classify these images into different pathology classes.

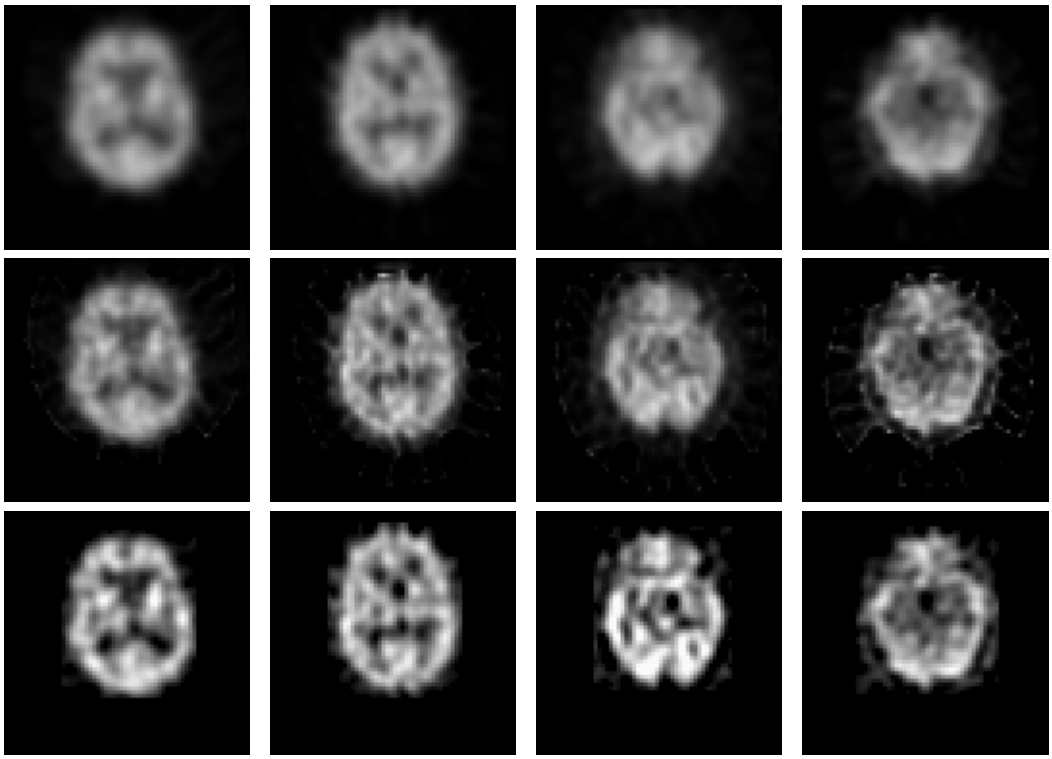

Figure 4. Examples of brain SPECT image deconvolutions. Top: original images. Middle: deconvolution results of the LR's algorithm after 200 iterations (as chosen by the proposed stopping rule). Bottom: deconvolution results of the NAS-RIF algorithm based on the proposed support-finding algorithm.

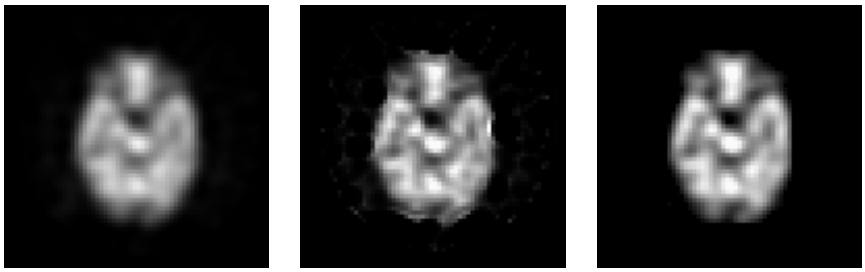

Figure 5. Examples of phantom SPECT image deconvolutions. (**a**) Original image. (**b**) LR's method, (**c**) NAS-RIF algorithm.

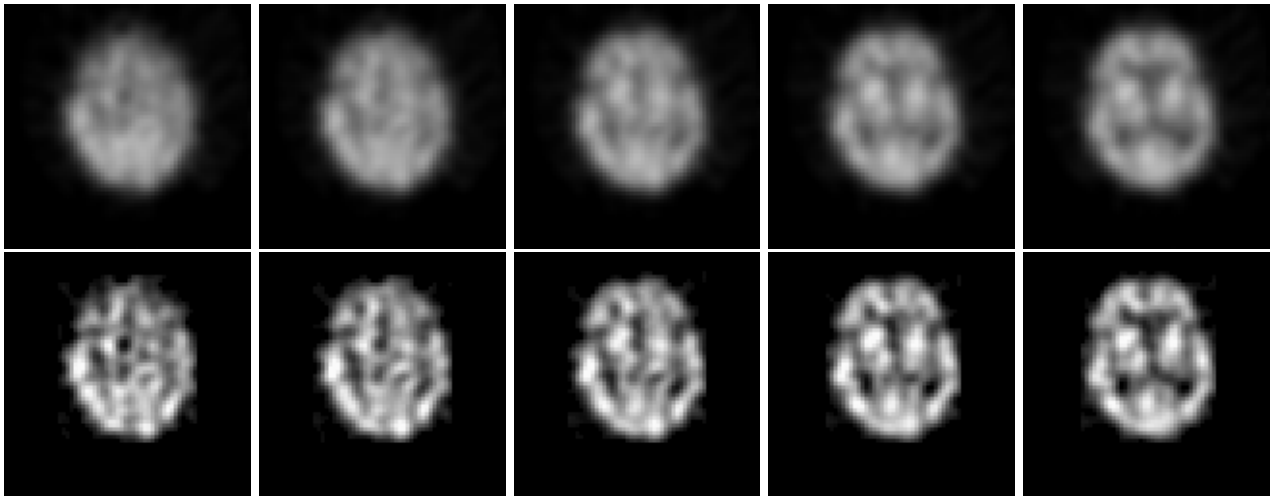

Figure 6. Examples of brain cross-sectional SPECT image deconvolutions given by the NAS-RIF algorithm combined with the proposed support-finding algorithm. Top: five consecutive real cross-sectional SPECT slices. Bottom: deconvolution results.

ACKNOWLEDGMENTS

The authors thank INRIA (Institut National de la Recherche en Informatique et Automatique, France) for financial support of this work (postdoctoral grant). The authors are also grateful to Jean-Paul Soucy and Christian Janicki (CHUM, University of Montreal) for having provided the SPECT images.

REFERENCES

1. L.B. Lucy. An iterative technique for the rectification of observed images. *The Astronomical Journal*, 79(6):8–37, 1974.
2. D. Kundur and D. Hatzinakos. Blind image restoration via recursive filtering using deterministic constraints. In *Proc. International Conference on Acoustics, Speech, and Signal Processing*, volume 4, pages 547–549, 1996.
3. M.T. Madsen and C.H. Park. Enhancement of SPECT images by Fourier filtering the projection set. *Journal of Nuclear Science*, 26:2687–2690, 1979.
4. T.S. Curry, J.E. Dowdey, and R.C. Murry. *Christensen's Physics of Diagnostic Radiology.* Lea and Febiger, 1990.
5. D.C. Costa and P.J. Ell. *Brain Blood Flow in Neurology and Psychiatry.* Series Editor: P.J. Ell, 1991.
6. B. Braathen, P. Masson, and W. Pieczynski. Global and local methods of unsupervised Bayesian segmentation of images. *Graphics and Vision*, 2(1):39–52, 1993.
7. S. Geman and D. Geman. Stochastic relaxation, Gibbs distributions and the Bayesian restoration of images. *IEEE Trans. on Pattern Analysis and Machine Intelligence*, 6(6):721–741, 1984.
8. J. Besag. On the statistical analysis of dirty pictures. *Journal of the Royal Statistical Society*, B-48:259–302, 1986.
9. S. Banks. *Signal processing, image processing and pattern recognition.* Prentice Hall, 1990.
10. A.P. Dempster, N.M. Laird, and D.B. Rubin. Maximum likelihood from incomplete data via the EM algorithm. *Royal Statistical Society*, pages 1–38, 1976.
11. S. Webb, A.P. Long, R.J. Ott, M.O. Leach, and M.A. Flower. Constrained deconvolution of SPECT liver tomograms by direct digital image restoration. *Med. Phys.*, 12(1):53–58, 1985.
12. K.J. Friston, J. Ashburner, C.D. Frith, J.B. Poline, J.D. Heather, and R.S.J. Frackowiak. Spatial registration and normalization of images. *Human Brain Mapping*, 3(3):165–189, 1995.